nature nanotechnology

SUPPLEMENTARY INFORMATION

DOI: 10.1038/NNANO.2011.217

Local electrical potential detection of DNA by nanowire-nanopore sensors

Ping Xie, Qihua Xiong, Ying Fang, Quan Qing & Charles M. Lieber

This file includes:

Methods

Silicon nanowire synthesis and nanowire-nanopore FET device fabrication. Silicon nanowires were synthesized using the Au-nanoparticle-catalyzed chemical vapor deposition (CVD) described previously[1,2]. 30 nm diameter gold nanoparticles (Ted Pella Inc.) were dispersed on the 600 nm silicon oxide coated silicon wafer (NOVA Electronic Materials Inc.). p-type silicon nanowires were synthesized at 435°C and 30 torr, with 2.4 standard cubic centimeters per minute (sccm) pure silane as silicon source, 3 sccm diborane (100 ppm in helium) as the boron dopant source, and 10 sccm argon as carrier gas. The nominal doping ratio is 4000:1 (Si:B), the growth time is 20 minutes and the diameter of silicon nanowires ranges from 30 – 50 nm. Silicon nanowires were dispersed onto 50 nm thick 100 μm × 100 μm silicon nitride TEM membrane grids (SPI supplies), and then electron beam lithography and Ni evaporation (60 nm) were used to fabricate ~1 μm spaced source and drain electrodes as described previously[1,2]; the electrodes were passivated with 75–100 nm silicon nitride deposited by plasma enhanced CVD. After lift-off, the chip was annealed in forming gas (H_2:N_2 10:90) at 380°C for 135 seconds (HeatPulse 610, Total Fab. Solutions) to reduce the Si-channel length by conversion to metallic NiSi[3]; these conditions typically yielded ≤ 200 nm channel. The nanowire-nanopore FET chip was cleaned using a UV-ozone stripper (Samco International Inc.) at 150 °C for 25 min on each side before loading into a field emission TEM (JEOL 2010F, 200kV), and then ~10 nm diameter nanopores were formed using a convergent beam[4] at the desired nanopore location for 2–5 minutes. Following TEM, the chip was cleaned using the UV-ozone stripper at room temperature for 25 min on each side to remove carbon deposition. Last, the chip was annealed in forming gas at 250 °C – 350 °C for 30 s.

SGM characterization. Nanowire-nanopore FET devices were characterized in the dry state by SGM using a Nanoscope IIIa Multi-Mode AFM (Digital Instruments Inc.). A conductive AFM tip (Nanosensors Inc.) was biased at -10 V and scanned 20 nm above the surface, and the conductance change of the nanowire-nanopore FET was recorded as a function of the tip position as described previously[5]. The SGM conductance change profile of the nanowire-nanopore FET was taken along the nanowire by averaging the conductance map over the apparent width (~100 nm) of nanowire perpendicular to the nanowire axis (by WSxM software[6]). This conductance change profile then was converted into sensitivity profile by dividing the conductance change by

the tip voltage.

Solution measurement setup. Prior to final assembly of the nanowire-nanopore sensor apparatus, the device chip was cleaned in the UV-ozone stripper at room-temperature for 25 min each side, and the chip was glued in the center recess in a home-made PCB chip carrier using Kwik-Cast^{TM} silicone glue (World Precision Instruments, Inc.). The depth of the recess made the active device surface flush with the surface of the rest of PCB board. The *cis* and *trans* PDMS chambers were cleaned using an ultrasonic cleaner sequentially in deionized (DI) water, 70% ethanol and pure ethanol for 30 min, and finally stored in pure ethanol. Prior to assembly the chambers were heated at 80 °C for ~2 hours, and then mounted and mechanically-clamped to the chip/chip carrier (see Fig. S1). In a typical measurement, the *trans* chamber (device side) was filled with 10 mM buffer (10 mM KCl + 0.1x TAE buffer (4 mM tris-acetate and 0.1 mM EDTA)) solution, and the *cis* chamber was filled with 1 M buffer (1 M KCl + 1x TAE buffer (40 mM tris-acetate and 1 mM EDTA)). All solutions were sterilized, degassed, and filtered by 20 nm Anotop syringe filter (Whatman Ltd.) before use.

DNA solution preparation. Commercial pUC19 vector (New England BioLabs Inc.) was linearized with SmaI (New England BioLabs Inc.), and purified by QIAquick® PRC purification kit (QIAGEN). The resulting DNA concentration was characterized by UV-Vis absorption at 260 nm, and the linear pUC19 solution was diluted to ~30 nM in 0.1× TAE buffer and stored at -20 °C as 30 μL aliquots. DNA solutions were further diluted to desired concentration in 1 M measurement buffer (see Solution measurement setup section above) immediately before experiments.

Nanowire-nanopore electrical measurements. The ionic current signals were recorded with Axopatch^{TM} 200B patch-clamp amplifier (Molecular Devices, Inc.) with $\beta = 0.1$ (10^8 gain) and 2 kHz bandwidth. Nanowire-nanopore FETs conductance values were measured at 150 mV source-drain voltage. The FET source-drain currents were amplified by DL 1211 current amplifiers (DL Instruments) with 10^6 gain and 0.3 msec rise time. The ionic current and FET signals were digitized (1440A, Molecular Devices, Inc.) and recorded at 5 kHz. The 1440A digitizer was also used to provide the source-drain voltage and trans-membrane voltage (all voltages specified below are trans-membrane voltage unless otherwise noted). All measurements

were performed in a home-build dark Faraday box. FETs, current amplifiers and digitizer are grounded to the building ground.

Buffer concentration distribution. A model (Fig. S2) similar to the literature[7] was used to analyse the concentration distribution between the distinct bulk *cis* and *trans* chamber buffer concentration. To implement a rough analytical calculation and examine relevant physical trends, we made several approximations, including (1) the nanowire-nanopore FET was treated as a point potential detector, (2) the concentration distribution is assumed to be determined only by the steady state diffusion driven by the *cis* / *trans* concentration difference, (3) the surface charge of SiN_x membrane and silicon nanowire can be ignored at the experimental ionic strength, and (4) the buffer concentration distribution and potential can be approximated as constant in the small hemispheres on both sides of the nanopore (shaded parts, Fig. S2). For steady state conditions the diffusion equations are then given as:

$$\begin{cases} \dfrac{\partial C}{\partial t} = 0 & \text{(For both chambers and inside the NP)} \\ r\dfrac{\partial^2 C(r)}{\partial r^2} + 2\dfrac{\partial C(r)}{\partial r} = 0 & \text{(For both chambers)} \\ \dfrac{\partial \mathrm{C(z)}}{\partial \mathrm{z}} = const & \text{(Inside the NP)} \end{cases} \quad (1)$$

For the *cis* chamber far away from the nanopore, $C = C_{Cis}$, for the *trans* chamber far away from the nanopore, $C = C_{Trans}$, and assuming concentration continuity at the nanopore openings at both chambers we obtain

$$\begin{cases} C_C(r) = C_{Cis} - \dfrac{C_{Cis} - C_{Trans}}{4(2l+d)}\dfrac{d^2}{r} & (Cis \text{ chamber}) \\ C_T(r) = C_{Trans} - \dfrac{C_{Trans} - C_{Cis}}{4(2l+d)}\dfrac{d^2}{r} & (Trans \text{ chamber}) \\ C_P(z) = C_{Trans} + \dfrac{C_{Cis} - C_{Trans}}{2(2l+d)}(4z+d) & \text{(NP)} \end{cases} \quad (2)$$

where C_C, C_T and C_P are the buffer concentration distribution in the *cis*, *trans* chambers and nanopore, respectively, and l and d are the membrane thickness and nanopore diameter, respectively.

Potential change at the nanowire-nanopore detector. The solution conductivity, σ, is ca.

proportional to the buffer concentration in the concentration range of our experiments and can be expressed as

$$\sigma = \sum \cdot C \tag{3}$$

where Σ is the molar conductivity of the solution. For a total current I the potential drop can be written as:

$$\begin{cases} dV_C(r) = \dfrac{I dr}{2\pi\Sigma C_C(r) r^2} & (Cis \text{ chamber}) \\ dV_T(r) = \dfrac{-I dr}{2\pi\Sigma C_T(r) r^2} & (Trans \text{ chamber}) \\ dV_P(r) = \dfrac{4 I dz}{\pi\Sigma C_P(z) d^2} & (\text{NP}) \end{cases} \tag{4}$$

where V_C, V_T and V_P are the potential distributions in the *cis*, *trans* chambers and nanopore respectively. Given that far away from nanopore *cis* and *trans* chamber potentials are the applied voltage and 0, respectively, we obtain:

$$\begin{cases} V_C(r) = V + \dfrac{2I(2l+d)}{\pi\Sigma(C_{Cis} - C_{Trans})d^2} \ln(1 - \dfrac{(C_{Cis} - C_{Trans})d^2}{4(2l+d)C_{Cis} r}) \\ V_T(r) = \dfrac{2I(2l+d)}{\pi\Sigma(C_{Cis} - C_{Trans})d^2} \ln(1 + \dfrac{(C_{Cis} - C_{Trans})d^2}{4(2l+d)C_{Trans} r}) \\ V_P(r) = \dfrac{2I(2l+d)}{\pi\Sigma(C_{Cis} - C_{Trans})d^2} \ln(\dfrac{(4l+d)C_{Trans} + dC_{Cis} + 4(C_{Cis} - C_{Trans})z}{2(2l+d)C_{Trans}}) \end{cases} \tag{5}$$

Since the potential is continuous at both nanopore openings and the total voltage applied is V, the equations can be further simplified:

$$\begin{cases} V_C(r) = V + \dfrac{V}{\ln(C_{Cis}/C_{Trans})} \ln(1 - \dfrac{d^2(1 - C_{Trans}/C_{Cis})}{4(2l+d)r}) \\ V_T(r) = \dfrac{V}{\ln(C_{Cis}/C_{Trans})} \ln(1 + \dfrac{d^2(C_{Cis}/C_{Trans} - 1)}{4(2l+d)r}) \\ V_P(r) = \dfrac{V}{\ln(C_{Cis}/C_{Trans})} \ln(\dfrac{4l + d + dC_{Cis}/C_{Trans} + 4(C_{Cis}/C_{Trans} - 1)z}{2(2l+d)}) \end{cases} \tag{6}$$

and the electric field inside nanopore is:

$$E_P(r) = \frac{dV_P(r)}{dz} = \frac{4V(C_{Cis}/C_{Trans} - 1)}{\ln(C_{Cis}/C_{Trans})} \frac{1}{4l + d + dC_{Cis}/C_{Trans} + 4(C_{Cis}/C_{Trans} - 1)z} \tag{7}$$

The potential change signal distribution in the *trans* chamber during DNA translocation can be

estimated from the reduction in cross-sectional area by a the DNA:

$$\delta V_T = \frac{\partial V_T}{\partial A}\delta A = \frac{2\delta AV}{\pi \ln(C_{Cis}/C_{Trans})}\frac{(4l+d)(C_{Cis}/C_{Trans}-1)}{(2l+d)(d^2(C_{Cis}/C_{Trans}-1)+4(2l+d)r)} \quad (8)$$

Here δA is the cross-sectional area of dsDNA. This result is equation (1) in the main text. This signal at the *trans* chamber nanopore opening (where the nanowire-nanopore FET resides) during DNA translocation can be estimated by setting r in equation (8) to $d/2$:

$$\delta V_T\big|_{d/2} = \frac{2\delta AV}{\pi \ln(C_{Cis}/C_{Trans})}\frac{(4l+d)(C_{Cis}/C_{Trans}-1)}{(2l+d)(d^2(C_{Cis}/C_{Trans}+1)+4ld)} \quad (9)$$

The validity of this mechanism depends on the linear increasing of solution resistivity at lower salt concentration around the nanopore. However, since both SiN_x and DNA are negatively charged under normal pH condition, there will be positive counter ions around the nanopore, which contribute to conduction and limit further increases in solution resistivity at very low salt concentration. An upper limit for the solution resistivity around a nanopore has been previously reported to happen when the salt concentration is lower than ~0.3 - 0.4 M[8], which should set a lower limit for the effective or average buffer salt concentration in our potential sensing mechanism. Interestingly, experiments designed to test the lower ionic strength limits (P.X. & C.M.L., *unpublished results*), we find that when $(C_{Cis}+C_{Trans})/2$ is ~0.3 – 0.4 M that we experience pore clogging.

Ratio of the FET and ionic current signals. The resistance of the system can be obtained using the voltage drop across the chambers and nanopore as:

$$\begin{cases} R_{Cis} = \dfrac{-2(2l+d)}{\pi\Sigma(C_{Cis}-C_{Trans})d^2}\ln\left(1-\dfrac{(C_{Cis}-C_{Trans})d}{2(2l+d)C_{Cis}}\right) \\ R_{Trans} = \dfrac{2(2l+d)}{\pi\Sigma(C_{Cis}-C_{Trans})d^2}\ln\left(1+\dfrac{(C_{Cis}-C_{Trans})d}{2(2l+d)C_{Trans}}\right) \\ R_{Pore} = \dfrac{2(2l+d)}{\pi\Sigma(C_{Cis}-C_{Trans})d^2}\ln\left(\dfrac{(4l+d)C_{Cis}+dC_{Trans}}{(4l+d)C_{Trans}+dC_{Cis}}\right) \end{cases} \quad (10)$$

where the total resistance and ionic current are:

$$\begin{cases} R = R_{Cis}+R_{Trans}+R_{Pore} = \dfrac{2(2l+d)}{\pi\Sigma(C_{Cis}-C_{Trans})d^2}\ln\left(\dfrac{C_{Cis}}{C_{Trans}}\right) \\ I = V/R = \dfrac{\pi\Sigma(C_{Cis}-C_{Trans})d^2V}{2(2l+d)\ln(C_{Cis}/C_{Trans})} \end{cases} \quad (11)$$

The ionic current signal due to DNA translocation can be written as:

$$\delta I = \frac{\partial I}{\partial A}\delta A = \frac{(C_{Cis} - C_{Trans})(4l + d)V\Sigma}{\ln(C_{Cis} / C_{Trans})(2l + d)^2}\delta A \tag{12}$$

We can see that both potential change signal and ionic current signal depend on voltage, although their ratio is a constant for a given buffer concentrations

$$\frac{\delta V_T}{\delta I} = \frac{2(2l + d)}{\pi d(dC_{Cis} + (4l + d)C_{Trans})\Sigma} \tag{13}$$

Bandwidth estimation. The intrinsic bandwidth of the potential change signal can be estimated by the nanopore RC bandwidth. We first analyse the signal distribution around the nanopore: In the *cis* chamber, the potential around the nanopore can be regarded as a constant due to the high salt concentration (see Fig. S3), while in the *trans* chamber, the potential signal is highly localised around the nanopore and decays as $1/r$ when r is large (equation (8)). The characteristic decay length of the signal from equation (8) is:

$$\lambda = \frac{d^2(C_{Cis} / C_{Trans} - 1)}{4(2l + d)} \tag{14}$$

Due to the highly-localized nature of detector, we consider the signal within this decay length. The effective cross-membrane solution coupling capacitance C for this local signal will be the cross-membrane capacitance within the radius of decay length λ. The potential outside this range will not affect the signal because (i) of the small FET detector size and (ii) the potential outside this detector is ca. fixed to zero by the solution electrode. Hence, when the local potential change causes charging or discharging, the charging current at any point within the decay length passes through two parallel pathways; these are through the solution in *trans* chamber directly to the solution electrode and through the solution in nanopore and then the solution in *cis* chamber to the other solution electrode. Focusing on the dominant second path, and using the total solution resistance R in equation (11) as a conservative upper limit for the solution resistance, yields a lower estimate for the potential signal RC bandwidth, BW :

$$BW = \frac{1}{2\pi RC} = \frac{l}{2\pi^2 R\varepsilon\varepsilon_0\lambda^2} \tag{15}$$

where ε and ε_0 are relative dielectric constant of SiN_x membrane and vacuum dielectric constant, respectively. This estimation is based on the steady-state diffusion such that the bandwidth is

limited by the KCl diffusion time across the membrane: $\sim l^2/2D$, where D is the diffusion coefficient. For signals faster than diffusion time, the potential change signal calculation should be based on the change of nanopore effective area for a constant salt concentration distribution. In this case, a similar calculation shows that the potential change signal follows the same characteristic decay length as equation (14), and thus that the bandwidth estimate in equation (15) is essentially unchanged. The RC bandwidth plotted as a function of nanopore diameter and solution concentration ratio (Fig. S4) shows that the bandwidth decreases with increasing concentration ratio, which can be understood in terms of the increasing decay length and corresponding capacitance. Importantly, for this mechanism the bandwidth increases with decreasing nanopore diameter. This key result arises from the fact that the decrease in decay length associated with a smaller nanopore dominates over the increase in solution resistance.

Analysis of translocation events. The translocation events were indentified and analysed using a MatLab (MathWorks®) program. Falling and rising event edges were found by the program when the change of signal within 0.2 msec was larger than 6 times the baseline standard deviation. After falling and rising edges were defined, we used well-defined and separated events based on the criteria (i) the event duration is at least 1 msec and (ii) the separation between the rising edge of event N and the falling edge of event N+1 is ≥1 msec. The error bars in Fig. 3e are standard deviations of the FET signal amplitude and standard deviations of FET signal / ionic current signal ratio, respectively, for all well-defined and separated events at a given voltage as defined above.

Control experiments using different buffer salt concentrations and uncharged polymers. To further test our local potential sensing mechanism, control experiments at different buffer salt concentrations were performed. First, translocation experiment was carried by raising the buffer concentration in both chambers by a factor of 3.3 from 1 M / 10 mM to 3.3 M / 33 mM. Data recorded on an independent chip with three nanowire-nanopore devices and nanopore diameters of ~10 nm (Fig. S6) exhibit correlated translocation events between the total ionic current events and the individual FET channels. This behavior is very similar to the data shown in Figure 4. Second, translocation experiments were also carried out with the *cis / trans* concentrations of 3.3 M / 330 mM, such that the overall concentration gradient was reduced by a factor of 10 (from

100 to 10). Similar correlated events between the total ionic current signal and the individual FET channels were again observed, although in this case the FET translocation event amplitudes were consistently smaller. To directly compare the FET signals in these two experiments (as well as compare the signals with the data in Fig 4), the individual nanowire-nanopore FET solution-gated transconductance values were determined and used to convert conductance signal amplitudes to potential change as described previously[9]. A summary of these results (Fig. S7) shows that the potential change signals for nanowire-nanopore FET devices are similar when the buffer concentration in both chambers change proportionally (i.e., 1M / 10 mM and 3.3 M / 33 mM) but decrease significantly when the buffer concentration ratio decreases (i.e., 3 M / 330 mM). These observations are in agreement with the predictions of our model. However, the similar signals observed for 1M / 10 mM and 3.3 M / 33 mM, are fundamentally different from the expectation for a conventional FET charge sensing mechanism in which any increase of buffer concentration will reduce the FET signal due to the shorter screening length. In this comparison, we exclude channel-3 FET in main Figure 4 because the long translocation times are indicative of contamination of this nanopore. Hence, the effective nanopore diameter could be much smaller than measured under TEM, which would preclude meaningful direct comparison (due to signal's dependence on nanopore diameter). In addition, we have carried out experiments with polyethylene glycol (PEG), which is a neutral polymer previously studied in translocation experiments[10], as an added test of our model. We note that PEG has a smaller effective cross-sectional area than dsDNA, and thus exhibits a smaller change ionic current during translocation[7,10]. Simultaneous recording of PEG translocation in ionic current and FET conductance shows a very similar correlated trace (Fig S8), although the signal amplitude in both channels are much smaller than we record for dsDNA. The smaller FET signal is consistent with expectations for our model, and moreover, quantitative comparison of the ratio of the nanowire-nanopore FET signal to ionic current signal for PEG vs. DNA translocation under these conditions (i.e., 3.3 M / 33 mM) demonstrates that the ratios are the same as predicted by our model for similar nanopore size devices (equation (13)). Significantly, the fact that PEG is neutral or slightly positively charged due to the cation coordination[10] and still yields the same signal polarity in FET channel is inconsistent with a charge-based FET sensing mechanism but in complete agreement with our potential sensing mechanism.

Reconstruction of the total ionic current from FET channels. To reconstruct the ionic current signal from the independently measured 3 nanowire-nanopore FET channels in Fig. 4b, we determined typical ionic current signal amplitude for each of the three nanopores by the distribution of ionic currents associated with each channel from the correlation of the independent FET signals and total ionic current. The typical ionic current signal amplitude for nanowire-nanopore FET-1, FET-2 and FET-3 were 3.35, 5.90 and 4.70 nA, respectively (measured from Fig. S9). Similarly, the typical total ionic current baseline can also be defined from the distribution of total ionic currents. The reconstruction (main Fig 4b, top panel red trace) is calculated by subtracting the corresponding typical ionic current signal amplitude from the typical baseline during every FET event in all three FET channels. In addition, the ionic current amplitudes for simultaneous translocation in nanopore-1 & nanopore-3 and nanopore-2 & nanopore-3 are 8.15 and 10.60 nA, respectively. These values differ from the simple summation of corresponding individual translocation current amplitudes within the error of the bin size (0.1 nA). This agreement further demonstrates the independence of all nanopores.

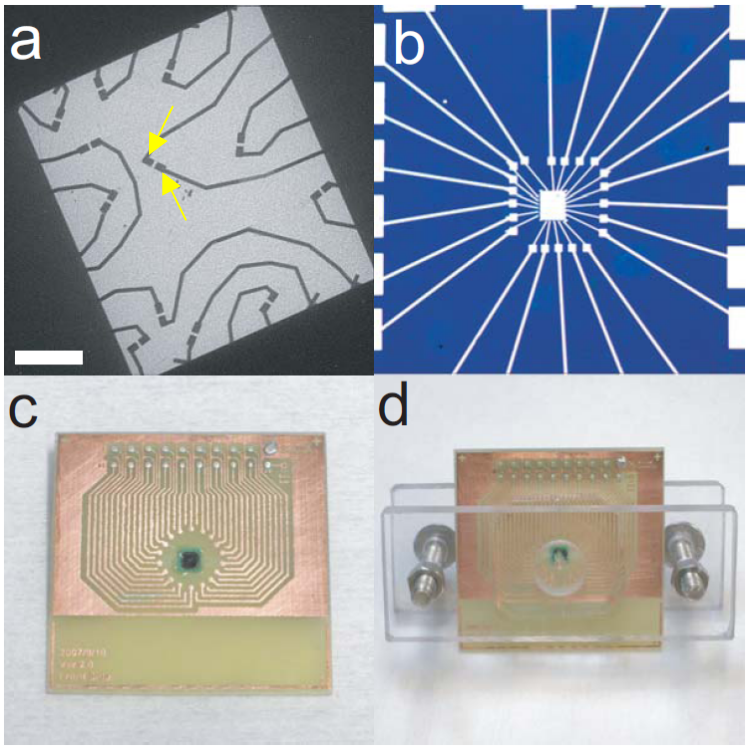

Supplementary Figure S1 | Images of representative devices. a. Low resolution TEM image of the central SiN_x membrane part of a nanowire-nanopore chip. Scale bar = 20 µm. The central bright rectangle is the suspended SiN_x membrane area with nanowire-nanopore FETs. Dark lines on the membrane are metal contacts. Yellow arrows point to the source and drain contact of a nanowire-nanopore FET (not visible in gap between two contacts). **b.** Optical image of the device side of the SiN_x membrane chip. Image size = 1.6 mm × 1.6 mm. The central bright rectangle is the suspended SiN_x membrane and bright stripes are metal lines connecting FET to the large metal wire-bonding pads visible on the edges of this image. **c.** Photograph of a home-made PCB chip carrier with a SiN_x membrane chip glued on. PCB board size = 4 cm × 4 cm. The central dark part is the SiN_x membrane chip. Bright metal lines on the chip carrier are copper, which are used to interface the devices to outside instrumentation. A few wire bonding wires are visible between the chip and copper lines. **d.** Photograph of a PCB chip carrier with assembled PDMS chambers.

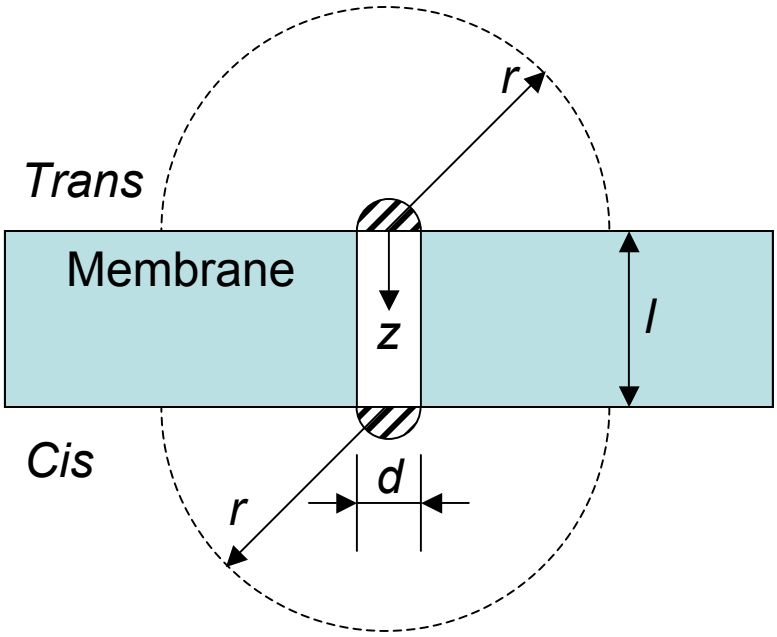

Supplementary Figure S2 | Geometry of calculation. The calculation is based on a cylindrical nanopore model. Here, *d* is the nanopore diameter, *l* is the membrane thickness, *r* is the distance to nanopore opening in solution chambers and *z* is the distance to nanopore opening on *trans* side inside the nanopore.

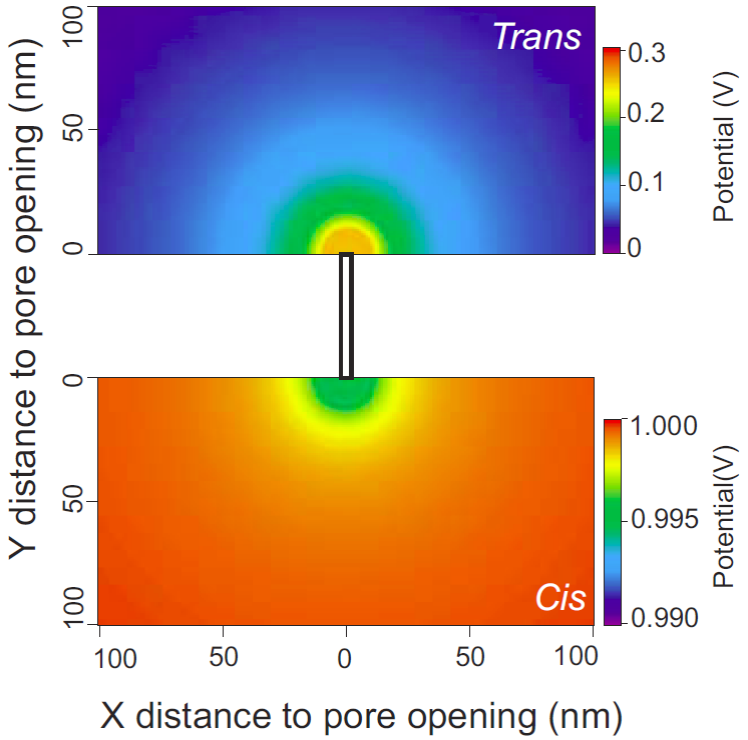

Supplementary Figure S3 | Potential distribution in *cis* and *trans* chambers. Calculated potential distribution in *cis* and *trans* chamber for a 10 nm diameter nanopore in 50 nm thick membrane at 1 V voltage. Buffer concentration ratio C_{Cis}/C_{Trans} is 100:1. The calculation is based on equation (6).

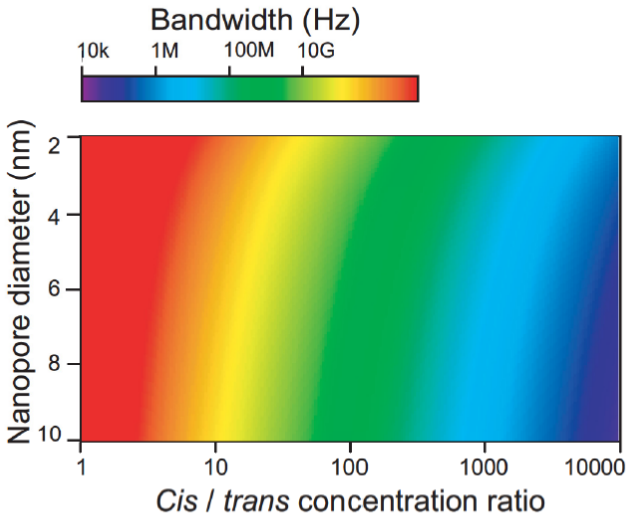

Supplementary Figure S4 | Estimated bandwidth of the potential signal. The calculation was made using supplementary equation (15) above as a function of buffer concentration ratio and nanopore diameter for a nanopore through a 50 nm thick SiN_x membrane. This bandwidth decreases with increasing concentration ratio, which can be understood in terms of the increasing decay length and corresponding capacitance. Importantly, the bandwidth also increases with decreasing nanopore diameter. This key result arises from the fact that the decrease in decay length associated with a smaller nanopore dominates over the increase in solution resistance.

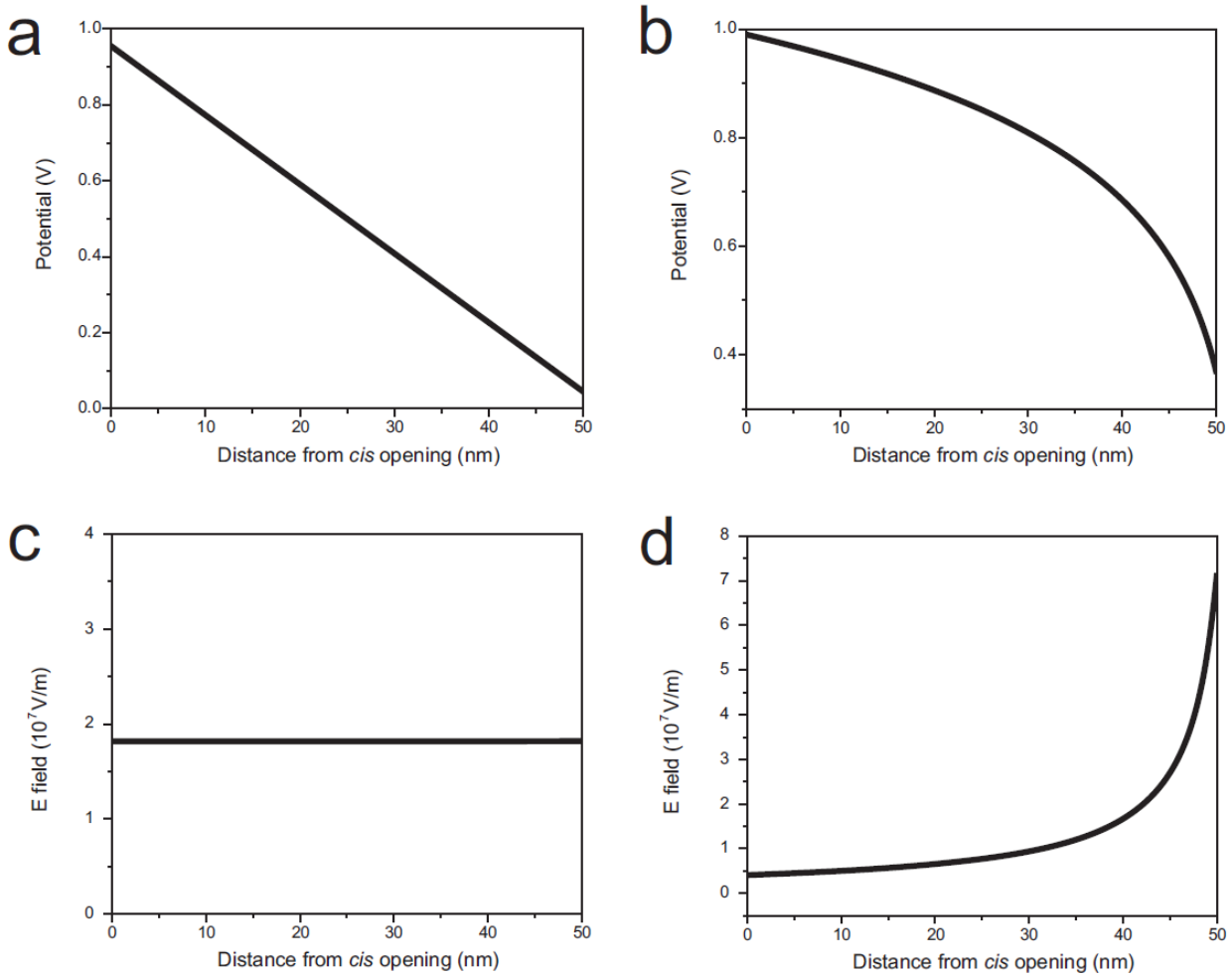

Supplementary Figure S5 | Potential and electric field distribution inside nanopore. a, and **b**, Potential distribution inside nanopore when *cis* / *trans* chamber buffer concentration ratio = 1:1 and 100:1 respectively. The calculation is based on equation (6). **c** and **d**, Electric field distribution inside nanopore when *cis* / *trans* chamber buffer concentration ratio = 1:1 and 100:1 respectively. The calculation is based on equation (7). Both calculations assume 50 nm thick SiN_x membrane, 10 nm diameter nanopore and 1 V voltage.

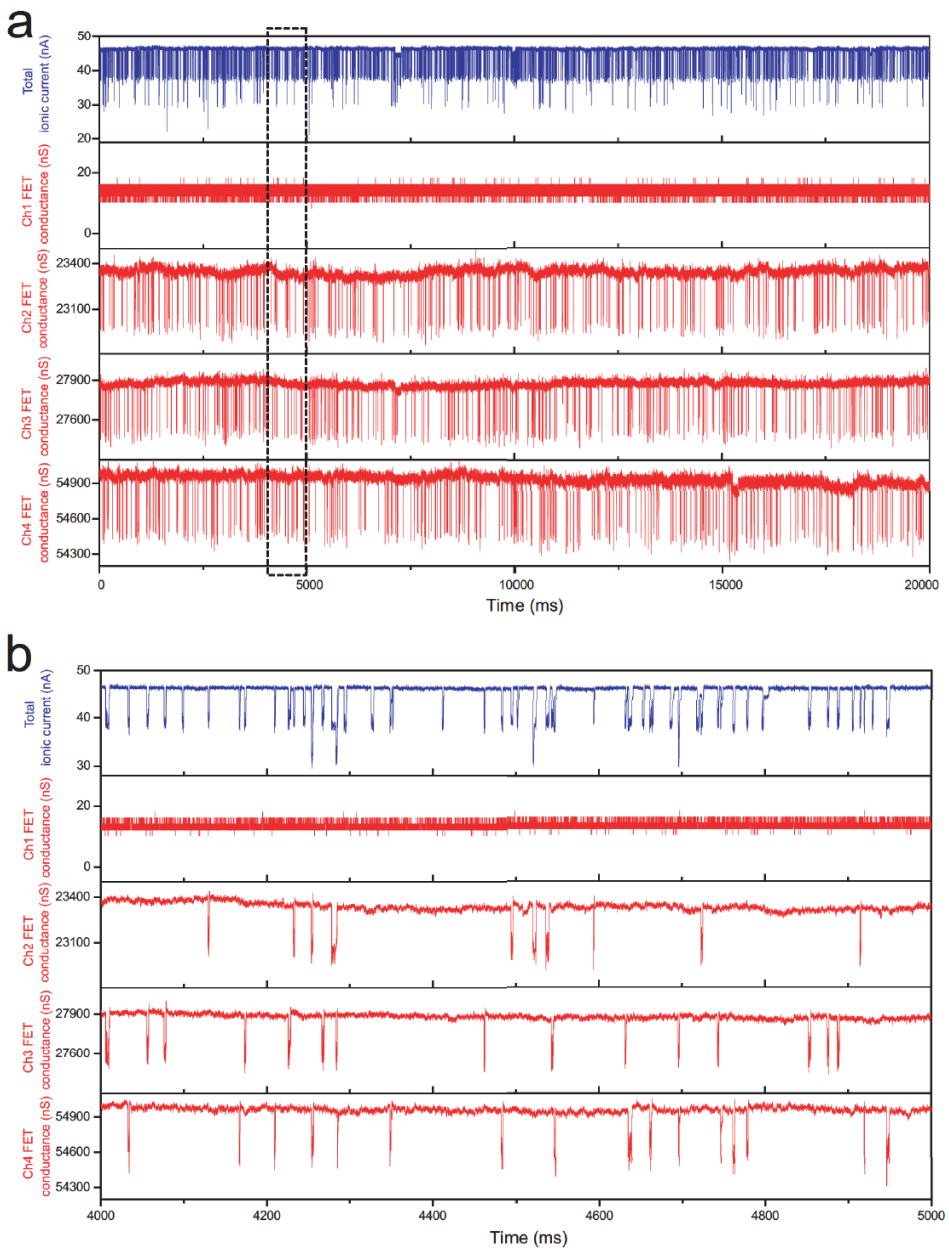

Supplementary Figure S6 | Translocation experiments at higher buffer salt concentration. Measurement is made with 3.3 M KCl buffer in *cis* chamber and 33 mM KCl buffer in *trans* chamber, voltage of 3 V and 1.4 nM pUC19 DNA. **a,** Simultaneous recording of the total ionic current and four nanowire-nanopore FET conductance channels. **b,** Higher time resolution view of the multiplexed recording from dashed rectangular area in panel **a.** In these experiments channel-1 FET failed before assembly, although the nanopore associated with this device remains open for DNA translocation. Hence, the conductance of channel-1 FET is zero and there are translocation events in total ionic current channel not associated with conductance signal from the remaining 3 FETs. The diameters of all three nanopores were all ~10 nm.

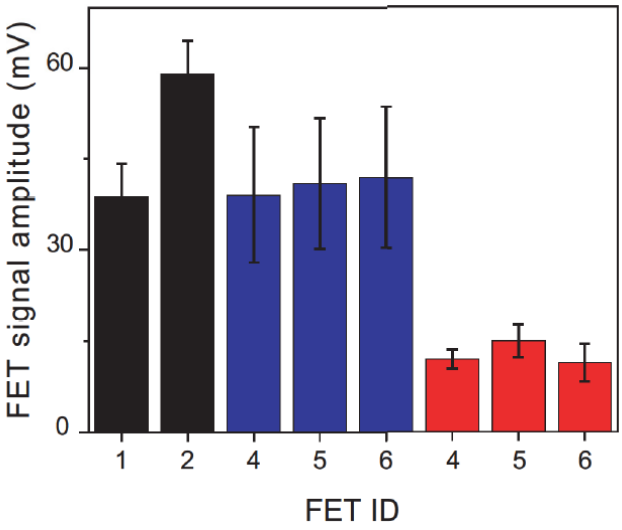

Supplementary Figure S7 | FET signal amplitude at different buffer concentrations. FET 1 and 2 are channel-1 and channel-2 FETs in main Figure 4; FETs 4, 5 and 6 are channel 2 – 4 FETs in supplementary Fig. S5, respectively. Black, blue and red indicate buffer concentration (*cis* chamber / *trans* chamber) at 1 M / 10mM, 3.3 M / 33mM and 3.3M / 0.33M respectively. The error bars denote ±1 standard deviation. All measurement are done at voltage = 3 V and 1.4 nM pUC19 in *cis* chamber. FET signal amplitude are converted from conductance signal to potential values as described in Methods. Devices show different signal amplitudes at different buffer concentration ratios, although the signal amplitude is approximately constant when the buffer concentration changes proportionally in both chambers. In this comparison, we exclude channel-3 FET in main Figure 4 because the long translocation times are indicative of contamination of this nanopore. Hence, the effective nanopore diameter could be much smaller than measured under TEM, which would preclude meaningful direct comparison (due to signal's dependence on nanopore diameter).

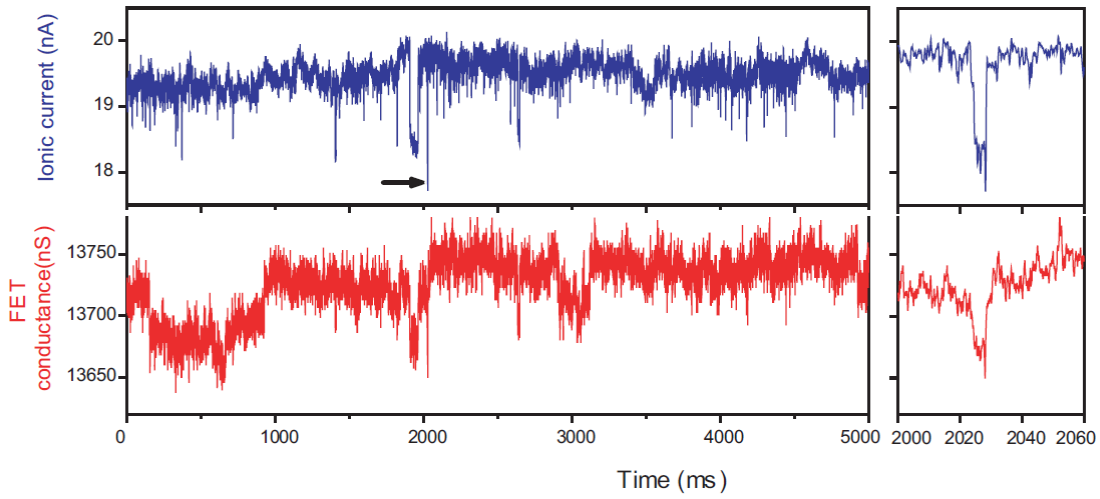

Supplementary Figure S8 | Neutral PEG translocation. Left panel: Simultaneously recorded ionic current (blue) and FET conductance (red) signals for PEG translocation. Right panel is the zoom-in view of a single translocation event at time indicated by the black arrow in left panel. Ionic current and FET conductance events are correlated. This trace is measured in 3.3 M / 33mM buffer (*cis / trans*), at 4 V voltage, and with 4.2 μM PEG (MW = 12000, from Alfa Aesar®) in front chamber (device side). Because PEG is significantly smaller than dsDNA, both ionic current and FET conductance signals are smaller than typical DNA signals. Both ionic current and FET signal amplitudes for short events appears smaller because limitations imposed by the recording bandwidth of ~1 kHz.

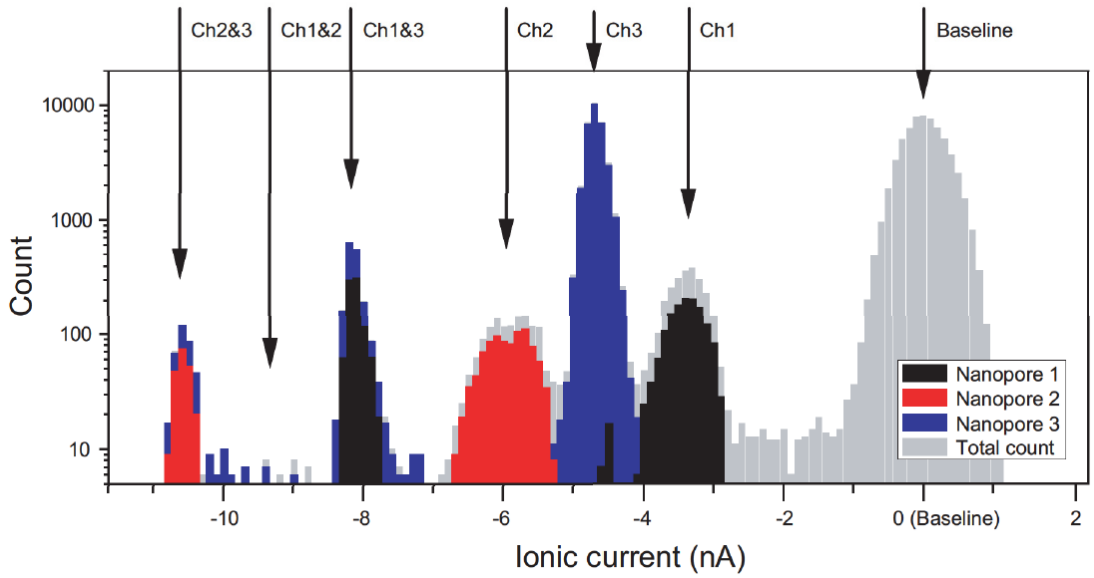

Supplementary Figure S9 | Channel specified histograms of ionic current in main Figure 4, panel a. Histogram of ionic current corresponding to dsDNA translocation through nanopores 1-3 are plotted in black, red and blue respectively and the histogram of the total ionic current is plotted in grey. The channel assignment is determined by the translocation signal in corresponding FET channel. The ionic current signal amplitude for each channel can be read directly from peak position indicated by black arrows in this figure.

Supplementary References

1. Cui, Y., Duan, X., Hu, J. & Lieber, C. M. Doping and electrical transport in silicon nanowires. *J. Phys. Chem. B* **104**, 5213-5216 (2000).
2. Cui, Y., Zhong, Z., Wang, D., Wang, W. U. & Lieber, C. M., High performance silicon nanowire field effect transistors. *Nano Lett.* **3**, 149-152 (2003).
3. Hu, Y., Xiang, J., Liang, G., Yan, H. & Lieber, C. M. Sub-100 nanometer channel length Ge/Si nanowire transistors with potential for 2 THz switching speed. *Nano Lett.* **8**, 925-930 (2008).
4. Kim, M. J., Wanunu, M., Bell, D. C. & Meller, A. Rapid fabrication of uniformly sized nanopores and nanopore arrays for parallel DNA analysis. *Adv. Mat.* **18** 3149-3153 (2006).
5. Yang, C., Zhong, Z. & Lieber, C. M. Encoding electronic properties by synthesis of axial modulation doped silicon nanowires. *Science* **310**, 1304-1307 (2005).
6. Horcas, I. *et al.* WSXM: A software for scanning probe microscopy and a tool for nanotechnology. *Rev. Sci. Instrum.* **78**, 013705 (2007)
7. Wanunu, M., Morrison, W., Rabin, Y., Grosberg, A. Y. & Meller, A. Electrostatic focusing of unlabelled DNA into nanoscale pores using a salt gradient. *Nat. Nanotech.* **5**, 160-165 (2009).
8. Smeets, R. M. M., *et al.* Salt dependence of ion transport and DNA translocation through solid-state nanopores. *Nano Lett.* **6**, 89-95 (2006).
9. Tian, B. *et al.* Three-dimensional, flexible nanoscale field-effect transistors as localized bioprobes. *Science* **329**, 831-834 (2005).
10. Reiner, J. E., Kasianowicz, J. J., Nable, B. J., Rovertson, J. W. Theory for polymer analysis using nanopore-based single-molecule mass spectrometry. *Proc. Natl. Acad. Sci., USA* **107**, 12080-12085 (2010).